Rapid Pneumatic Control of Bimodal, Hierarchical Mechanical Metamaterials

*Lance P. Hyatt and Ryan L. Harne**

Recent attention to pneumatically pressurized mechanical metamaterials has identified opportunity for large shape change and mechanical properties adaptation through the collective exploitation of reconfigurable internal structures and enclosed cavities. Yet, many of these ideas are found to act in smooth, continuous ways at moderate rate. This research explores a new class of bimodal, hierarchical mechanical metamaterials that exemplify rapid change of mechanical behavior by exploiting pneumatic pressure as a means to cross bifurcation. A lattice structure with periodic square cavities is presented as a model metamaterial to highlight important design considerations and mechanical behavior. An analytical model is formed to delineate the multimodal boundaries in a high-dimensional parameter space, while numerical simulations and experiments confirm the presence of each modal characteristic. The studies reveal the high rate of change afforded by this embodiment of pressurized mechanical metamaterials and confirm the origin lay in harnessing elastic instability. Extensions to the idea are compared against the Kutzbach–Grübler criteria to articulate how other metamaterial networks may be leveraged in this way. The outcomes of this research may inspire methods for high-rate shape and properties change via multimodal mechanical metamaterial assemblies, such as for soft robotic platforms.

1. Introduction

Mechanical metamaterials are engineered structures that exhibit mechanical properties not typically found in natural materials. These properties may include a negative Poisson's ratio (auxetic materials),[1,2] negative or anisotropic stiffness,[3–5] multistability,[6–8] and shape morphing.[9,10] With these unique mechanical behaviors, promising applications have been suggested including vibration isolation,[11] packaging and distribution,[12,13] deployable structures,[14] and mechanological systems.[15,16]

These behaviors are often facilitated by distinct deformation or collapse modes that arise from bifurcations associated with the periodic structure of the metamaterial.[17–21] In many cases, a single mode is present allowing for relatively simple methods to actuate a distinct response such as uniaxial compression. Several methods exist to program or tune the behavior of these structures, including changing internal void shapes,[22,23] altering the width of ligaments,[24] and functional grading.[25] When a structure exhibits multiple deformation modes, more complex control methods are necessary.[26] Recently, methods have been shown to use the rational design of structural geometry[27,28] or combinatorial design[29] to create multimodal structures that can be controlled with actuation methods such as biaxial or uniaxial compression. Many of the methods explored in previous works passively control the collapse of multimodal structures prior to any applied loading. This can limit the versatility of a metamaterial, since it would be incapable of adapting or tuning mechanical behavior during operation. Methods to exert both passive and active control of multimodal, multifunctional structures are still widely unexplored.

One method to govern such dynamic behavior in soft mechanical metamaterials is pneumatic pressurization.[3,30–32] By pressurizing networks of small channels, elastomeric structures have been designed that are capable of large deformations.[33] Recent work has shown how the mechanical properties such as the auxetic nature of a periodic metamaterial can be programmed through selective pressurization of internal cavities.[34] While the individual pressurization of cellular voids in metamaterials allows for a high level of tunability, the complexity of the actuation also increases. While capable of intricate motion, pneumatic pressurization is often limited by relatively slow actuation due to the need to move large volumes of air. There remains a need for simple pneumatic actuation methods that facilitate high-rate response in multimodal mechanical metamaterials. By devising such multimodal, pressurized metamaterials, means for rapid and large change of shape and properties would be afforded, as facilitated by a straightforward design of periodic, pressurized, and hierarchical cellular voids.

This research presents a class of bimodal, hierarchical metamaterials that exploit pneumatic pressurization of internal cavities to quickly control mechanical properties and shape reconfiguration. A model structure with periodic square cavities is examined to elucidate the fundamental principles that enable this response. Using an analytical model to capture the salient

L. P. Hyatt, R. L. Harne
Department of Mechanical Engineering
Pennsylvania State University
University Park, PA 16802, USA
E-mail: ryanharne@psu.edu

The ORCID identification number(s) for the author(s) of this article can be found under https://doi.org/10.1002/adem.202101375.
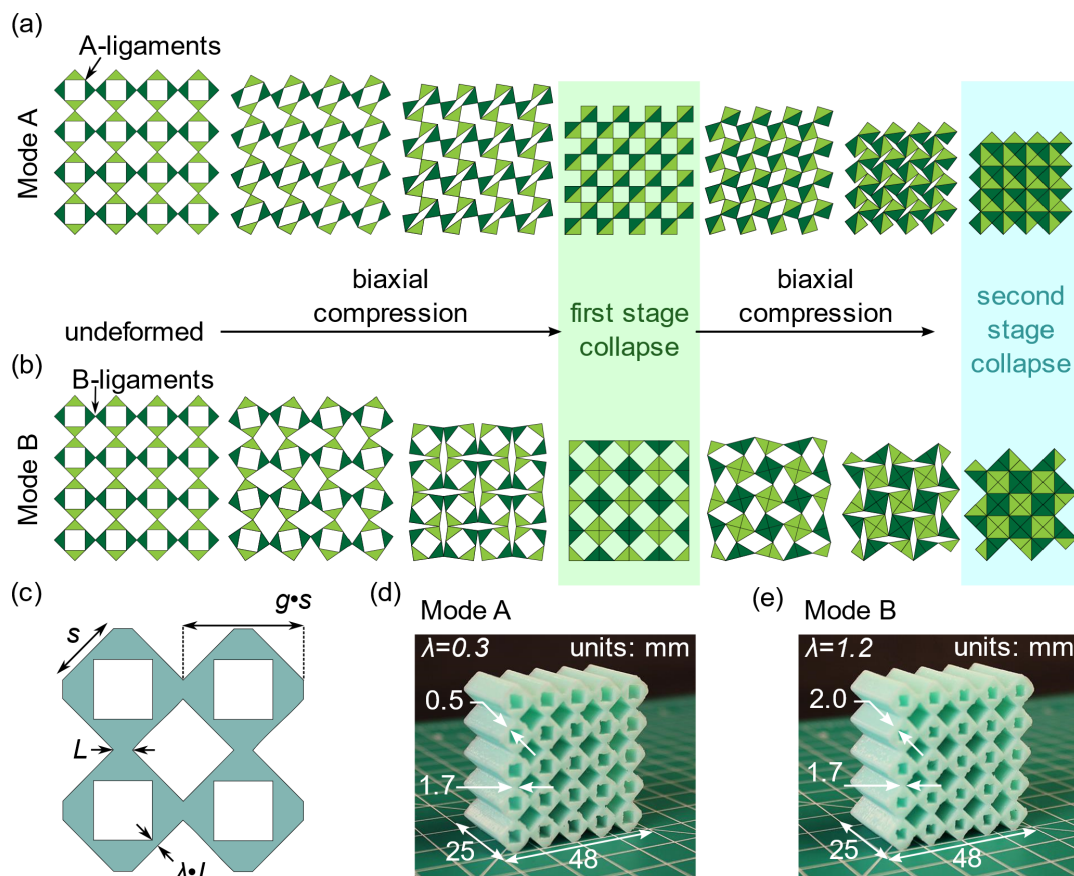
Figure 1. Exemplary collapse behavior for mode A and mode B of the bimodal metamaterial under biaxial compression. a) Mode A occurs when A-ligaments deform until self-contact (highlighted in green) and continues as B-ligaments deform until fully compact (light blue). b) Mode B occurs with B-ligaments collapsing first, then A-ligaments. c) Diagram showing design parameters of the physical model. Physical samples with ligament ratios of d) 0.3 and e) 1.2.

findings from numerical simulations and experiments, the onset of the bimodal collapse behavior in the model metamaterial shown in **Figure 1**a,b is investigated. Passive control of deformation is characterized through the modification of geometric parameters, and active control is demonstrated using single-channel pneumatic pressurization. It is shown experimentally that by applying or removing pressurization during collapse, the metamaterial can rapidly snap between the two deformation modes and corresponding soft and hard mechanical properties. This demonstrates the ability for real-time tuning of the metamaterial configuration and properties. Having characterized the phenomena for the model geometry, the rules that permit extensibility of the concept to other multimodal mechanical metamaterials are uncovered and tested.

2. Modal Description of Bimodal Metamaterial with Square Cavities

2.1. Ideal Kinematic Behavior

While many monomodal mechanical metamaterials are based on kinematic tilings with a single degree of freedom,[1] bimodal hierarchical metamaterials can be represented by kinematic tilings with multiple degrees of freedom. The design of a model metamaterial investigated in this paper is inspired by a single degree of freedom rotating squares pattern that reaches a fully compact configuration when subjected to biaxial loading[20] as seen in Figure S5a of Supporting Information. When a second, smaller square cavity is created in each solid square section, additional degrees of freedom are introduced. Section S3 of Supporting Information discusses how hierarchical cavities in periodic tilings may change the mobility of a metamaterial. Due to the additional mobility in the modified square pattern, the resulting collapse behavior is bimodal with two stages. Figure 1a,b shows the ideal, kinematic, zero-energy reconfiguration of the two modes under biaxial compression. Each mode is characterized by the order in which two sets of ligaments (A and B) bend during compression. The A-ligaments are located at the corners of the smaller square cavities as indicated in Figure 1a. Using the shading, A-ligaments exist at the intersection of the light and dark green triangular segments. Figure 1b shows the location of the B-ligaments at the corners of the larger square cavities where like colored triangles intersect.

Mode A (Figure 1a) occurs when the A-ligaments bend during the first stage of collapse, while the B-ligaments do not bend.

**ADVANCED
SCIENCE NEWS**

www.advancedsciencenews.com

**ADVANCED
ENGINEERING
MATERIALS**

www.aem-journal.com

Conversely, mode B (Figure 1b) occurs when the B-ligaments bend first, and the A-ligaments remain undeflected. For both collapse modes, the first-stage collapse continues until the metamaterial reaches self-contact which is highlighted in light green. In both cases, the resulting structure is a periodic tiling of square units similar to the original rotating squares pattern. Yet the subsequent biaxial load transfer differs markedly between the two collapse modes, since the square units of mode B are larger and rotated 45° compared to the units of mode A. With further biaxial compression, each mode has the second-stage collapse where the other set of ligaments begin to bend resulting in a completely compact configuration (highlighted in light blue). The biaxial compression is needed to ensure that the self-contact continues throughout the collapse. Under uniaxial compression, the contacting surfaces can slide past each other causing a disordered collapse.

In a mechanical metamaterial fabricated to cultivate such behavior, the soft modes are determined by the relative size of the A- and B-ligaments. The geometry of the structure is fully defined by the side length of the large cavities s, the spacing of each large cavity defined by a nondimensional geometric ratio g, and the ligament ratio λ, which is the ratio of the widths of the A-ligaments to the widths of the B-ligaments. These parameters are highlighted in Figure 1c. For a given geometric ratio, there exists a critical ligament ratio value which determines the modal collapse of the metamaterial. Metamaterials with ligament ratios smaller than the critical value exhibit mode A collapse, and larger ligament ratios cause mode B collapse. Section 3.1 outlines the derivation of the relationships used to calculate the critical ligament ratio with Equation (12). Figure 1d,e show two physical samples with a geometric ratio of 1.67 and ligament ratios of 0.3 and 1.2, respectively. The critical ligament ratio is 0.85. Therefore, the sample in Figure 1d exhibits mode A behavior, and the sample in Figure 1e exhibits mode B behavior.

2.2. Passive Control of Mechanical Properties

Physical samples are created using silicone rubber with a casting process described in Supporting Information Section S2. The samples are placed in a biaxial frame that converts uniaxial compression from a load frame (ADMET eXpert 5600) into biaxial compression as seen in **Figure 2**a,b. The biaxial frame is 3D-printed in acrylonitrile butadiene styrene plastic and exhibits a mechanical stiffness many orders of magnitude greater than that of the elastomeric mechanical metamaterials. The load frame lowers a rigid steel platen at a rate of 0.5 mm min^{-1} to examine the quasi-static response of the sample. The platen is attached to a load cell (PCB 110205A) to measure the applied force, while a laser displacement sensor (Micro-Epsilon optoNCDT ILD1750-200) measures the displacement of the load frame platen. Figure 2c shows the resulting mechanical properties in terms of the total sample reaction force according to the platen displacement of the top metamaterial surface. Photographs of common deformation moments from the experiments are highlighted in Figure 2d,e. The yellow dots in Figure 2c correspond to the stages highlighted in the photographs of Figure 2d,e.

The resulting curves in Figure 2c indicate that both collapse mode A (dark blue) and collapse mode B (light blue) exhibit two

pronounced collapse events. At points A_1 and A_2 (labeled in red), the first critical buckling point is reached. With increasing displacement, the material in both modes exhibits nearly zero stiffness until self-intersection is reached at points B_1 and B_2 (green). The models continue to compress until they reach the second critical buckling point at points C_1 and C_2 (dark blue). This secondary collapse results in another loading region with low stiffness until the fully compact configuration is reached at points D_1 and D_2 (cyan). The behaviors seen in Figure 2d,e closely match the ideal kinematic behavior (Figure 1a,b) and clearly demonstrates that the ligament ratio determines the mode that the material adopts under compression. Therefore, by tailoring the thicknesses of appropriate ligaments, engineers can exhibit passive control of the bimodal behavior of hierarchical metamaterials.

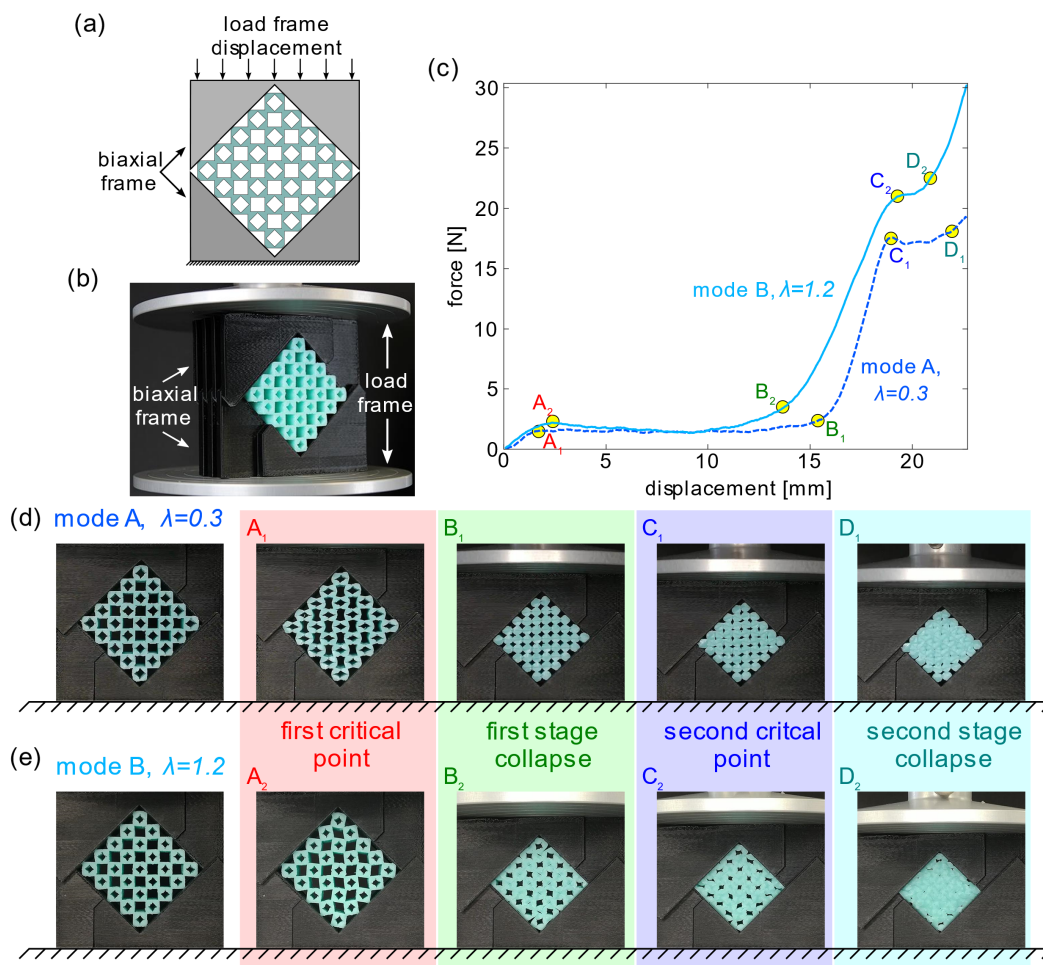## 3. Control of Collapse Behavior with Pneumatic Pressurization

The collapse modes of a bimodal hierarchical metamaterial are distinguished by which type of ligaments (A or B) bends before the other ligament type. In other words, under biaxial compression, the force on the structure increases until a critical buckling force is reached for one of the collapse modes. Therefore, to design a material that exhibits mode A or B, one must control the critical buckling loads for each mode. This can be done passively by changing the ligament ratio as seen in Figure 2d,e. With a ligament ratio of 0.3, the critical buckling load for mode A is less than mode B and the material exhibits mode A collapse. With a ligament ratio of 1.2, the critical buckling load for B is less than mode A resulting in mode B collapse.

It has been shown that applying sufficient pressure to an internal cavity controls the buckling of the outer walls under compression.[35] This principle can be used to actively control the deformation modes of hierarchical metamaterials by applying pneumatic pressure to select cavities. For the metamaterial in this paper, the added pressure to the smaller internal cavities creates resistance to the buckling of the A-ligaments forcing the material to enter collapse mode B. **Figure 3**a shows a two-dimensional cross section of the metamaterial under a biaxial compressive force F (red arrows) and a pressure applied to the smaller cavities (orange shaded region). It is assumed that the pressure and force are applied along the entire out-of-plane thickness.

3.1. Formulation of a Pseudo-Rigid-Body Model

To understand the relationship among the applied pressure, ligament ratios, and the collapse modes, a simple pseudo-rigid-body model (PRBM)[36] is created based on the collapse of smaller unit cells. A PRBM is often used in compliant mechanism design to accurately predict the behavior of flexible structures by modeling the flexible structure as rigid segments connected by revolute joints with torsional springs.

For a bimodal metamaterial, the deformation in each mode is highly localized to the bending ligaments. Therefore, a PRBM can be established for each deformation mode. Here, a PRBM is established for both mode A and mode B of the modified

ADVANCED
SCIENCE NEWS
www.advancedsciencenews.com

ADVANCED
ENGINEERING
MATERIALS
www.aem-journal.com

Figure 2. Demonstration of mechanical properties of bimodal metamaterial. a) Diagram of the biaxial frame converting uniaxial compression to biaxial compression, and a photograph with the 3D-printed frame b). The force–displacement relationship of both samples shown in Figure 1d–e. Photographs of deformation for the sample with ligament ratio of d) 0.3 showing collapse mode A (dark blue dashed), and e) 1.2 showing mode B (light blue solid). Labels in (d,e) correspond to points in the force–displacement curves in (c).
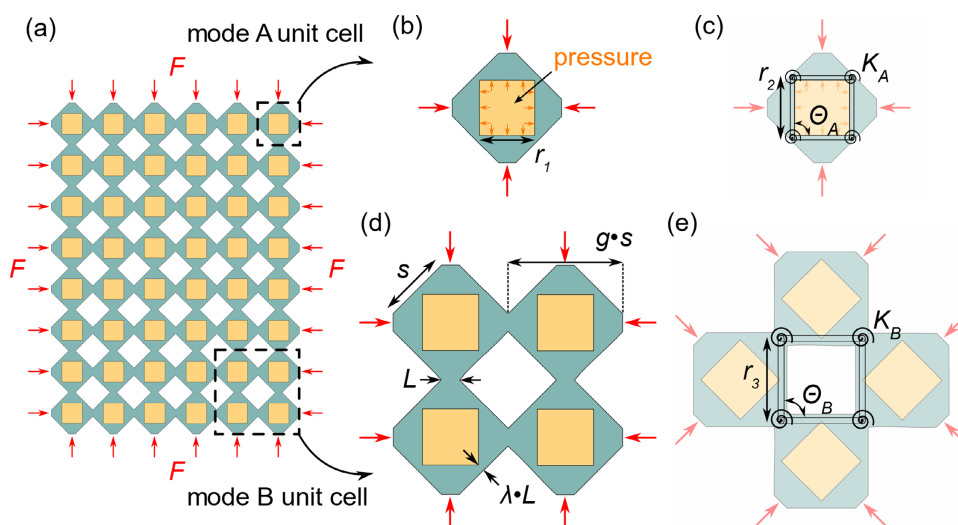
Figure 3. Unit cells of each mode under biaxial compression (red arrows) and applied pressure (orange). The pseudo-rigid-body model is shown for each mode unit cell (right). The PRBM for each cell is a four-bar mechanism with torsional springs at the location of the ligaments.

square tiling. Due to the periodic nature of the pattern, the collapse behavior can be fully characterized with a single unit cell. It is important to note that the two collapse modes do not share the same unit cell. The unit cell of mode A is shown in Figure 3b. The PRBM for mode A is shown in Figure 3c. The four A-ligaments are replaced with torsional springs located at the center of the ligament with spring constants of K_A. The springs are connected by four rigid links of length r_2. Conversely, Figure 3d shows the unit cell corresponding to mode B. For the PRBM of mode B in Figure 3e, the B-ligaments are replaced with torsional springs with spring constants K_B separated by rigid links of length r_3. Figure 3e has been rotated 45° to highlight the similarity to the PRBM of Figure 3c. Both modes feature a four-bar mechanism with four torsional joints, yet the relevant loading and geometries are distinct.

The lengths r_1, r_2, r_3, and L can be written as functions of the geometric ratio g, the ligament ratio λ, and the side length s

$$r_1 = s\left(g - \sqrt{2}\lambda g + 2\lambda - \frac{1}{\sqrt{2}}\right) \tag{1}$$

$$r_2 = s\left(g - \frac{\lambda g}{\sqrt{2}} + \lambda - \frac{1}{\sqrt{2}}\right) \tag{2}$$

$$r_3 = \frac{sg}{\sqrt{2}} \tag{3}$$

$$L = s(g - \sqrt{2}) \tag{4}$$

Using the PRBM for each mode, the principle of minimum potential energy is applied to determine the critical buckling load under biaxial compression. The complete formulation of the model for the modified square pattern is shown in Supporting Information Section S1.

For a metamaterial with a constant out-of-plane width w, the critical forces for mode A F_{crA} and mode B F_{crB} are

$$F_{crA} = \frac{K_A}{wr_2} + pr_1 \tag{5}$$

$$F_{crB} = \frac{K_B}{\sqrt{2}wr_3} \tag{6}$$

Here, it is seen that by increasing the applied pressure to the inner cavities, the critical load for mode A increases while the critical load of mode B is unaffected. By equating Equation (5) and (6) and solving for the pressure p, one obtains an expression for the threshold of pressure between modes A and B

$$p = \frac{K_B r_2 - \sqrt{2}K_A r_3}{\sqrt{2}wr_1 r_2 r_3} \tag{7}$$

The pressure obtained by Equation (7) indicates the pressure needed to cause the metamaterial to change collapse modes. If the B-ligament is significantly stiffer than the A-ligament ($K_B > K_A$), the material will exhibit mode A collapse. Yet if the pressure applied is greater than the value calculated in Equation (7), the material will collapse with mode B.

To design a metamaterial to exhibit mode A or mode B collapse using Equation (7), the torsional spring constants K_A and K_B need to be approximated. Meng et al.[16] developed a

model to approximate the torsional stiffness of a thin square ligament. The torsion stiffness of the ligament is found to be

$$K_\theta = \alpha Ewl^2 \tag{8}$$

where E is the Young's modulus, w is the out-of-plane thickness, l is the thickness of the ligament, and α is a nondimensional correction factor. For the A-ligaments investigated in this work, the spring constant is

$$K_A = \alpha_A Ew(\lambda L)^2 \tag{9}$$

The spring constant of the B-ligaments is

$$K_B = \alpha_B EwL^2 \tag{10}$$

To determine the values of the correction factors, finite element (FE) simulations are performed on individual ligaments subjected to bending. A full description of the method is given in the Supporting Information Section S1.1.

When Equation (9) and (10) are substituted into Equation (7), a nondimensional equation equal to the ratio of the applied pressure p to the Young's modulus E

$$\frac{p}{E} = \frac{L^2\left(\alpha_B r_2 - \sqrt{2}\alpha_A \lambda^2 r_3\right)}{\sqrt{2}r_1 r_2 r_3} \tag{11}$$

Solving Equation (11) for the ligament ratio yields an expression for the critical ligament ratio for any geometric ratio and applied pressure

$$\lambda = \sqrt{\frac{L^2 \alpha_B r_2 - \frac{p}{E}\left(\sqrt{2}r_1 r_2 r_3\right)}{\sqrt{2}L^2 \alpha_A r_3}} \tag{12}$$

From Equation (1)–(4), the lengths r_1, r_2, r_3, and L are proportional to the side length s and functions of the geometric ratio g and ligament ratio λ. Therefore, Equation (11) and (12) can be shown to be functions of the geometric and ligament ratios, and independent of the cavity side length. This independence means that the relationship between pressure ratio, geometric ratio, and ligament ratio is scalable to any size. Because the analytical model is based on the behavior of a single unit cell, it can be applied to any tiling of the square unit cells subject to biaxial compression.

It is important to note that this model assumes that there is only pure bending at the ligaments. Equation (11) and (12) neither account for expansion of the smaller cavities due to the applied pressure nor shearing or compression of the ligaments themselves.

3.2. Sealed Physical Samples for Pneumatic Pressurization

To implement pneumatic control in a physical model, airtight samples are created using a multistep fabrication method described in Supporting Information Section 2. The process seals and connects the inner cavities with a single channel allowing for an input of air pressure. Pictures of the sealed sample are shown in **Figure 4**a,b. The sealed samples have a greater out-of-plane width than the open samples to minimize the effects of the front and back faces, where the material that seals the cavities may otherwise mechanically influence the collapse behavior.
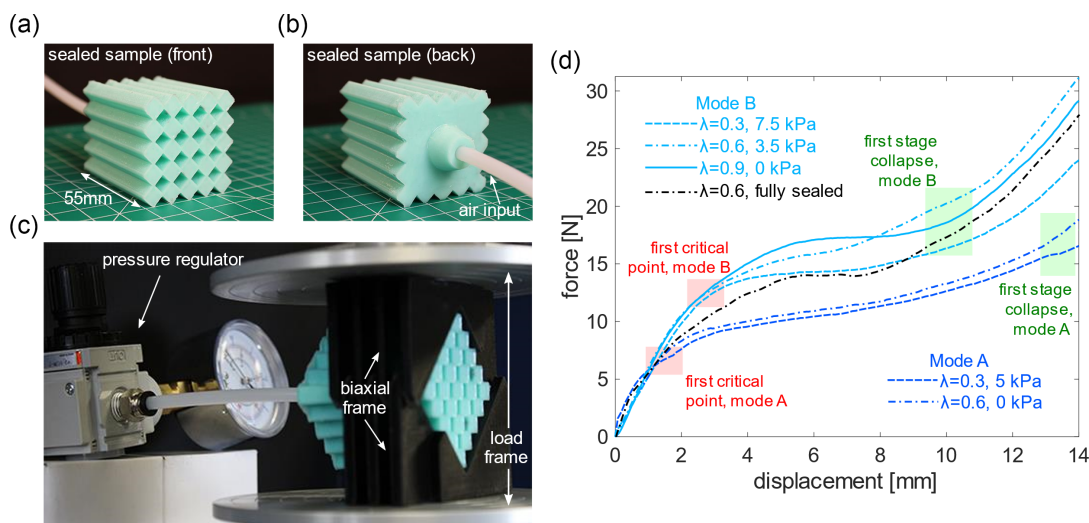
Figure 4. Experimental setup of pressurized samples. Photographs of the front a) and back b) of the sample showing the attached PE tube for air input. c) Sample in biaxial frame in load frame, connected to pressure regulator. d) Force–displacement curves for experimental results of pressurized samples. Dark blue indicates mode A, and light blue indicates mode B. Critical buckling regions (red) and first-stage collapse regions (light green) are highlighted.

The sealed samples are connected with a polyethylene (PE) tube to a pressure regulator (PneumaticPlus PPR2-N02BG-2) as seen in Figure 4c. The pressure regulator is connected to a pressurized air reservoir.

To show how the collapse modes differ with ligament ratio and pressure, three samples with ligament ratios of 0.3, 0.6, and 0.9 are tested over a range of pressures. All samples have a geometric ratio of 1.67. The samples are compressed to a vertical displacement of 15 mm with the same procedure as described in Section 2.2. This allows each sample to reach the end of the first stage of collapse, clearly indicating which mode is adopted. The resulting mechanical reaction forces during biaxial compression are shown in Figure 4d. The samples that exhibit mode A are shown in dark blue, while mode B collapse is indicated by light blue. Just as with the open samples, after the first critical load is reached (highlighted in red), the material exhibits low stiffness until it begins to self-contact as it finishes the first-stage collapse (highlighted in green). It is important to note that the samples with ligament ratios of 0.3 and 0.6 (dotted lines) which typically exhibit mode A collapse (dark blue) can exhibit collapse mode B (light blue) with small applied pressures of 7.5 and 3.5 kPa, respectively, as seen in Figure 4d.

The behavior of a fully sealed metamaterial is examined for comparison. This sealed metamaterial has a ligament ratio of 0.6 and does not have an opening for a PE tube so that air entrapped in the central voids does not escape during the biaxial compression and resulting internal collapse of the metamaterial network. The pressure in sealed cavities of the fully sealed metamaterial at the beginning of biaxial loading is atmospheric pressure, which is the same as for the remaining samples for which there is zero applied pressure. Therefore, the fully sealed sample begins exhibiting mode A collapse. When biaxial compression begins, the pressure in the fully sealed metamaterial increases acting like a pneumatic spring. The increase in pressure due to collapse is enough to make the sample follow mode B behavior as seen by the black dash-dotted curve in Figure 4d. Yet the fully
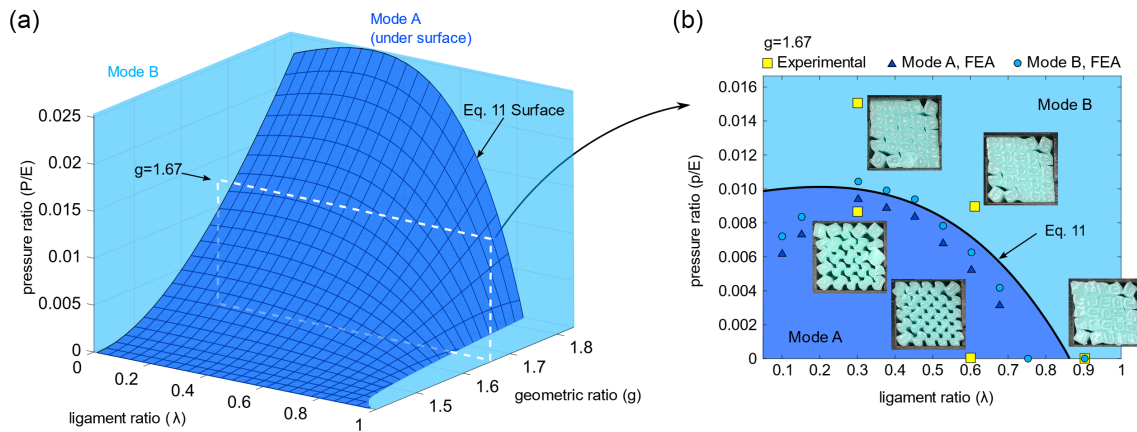
sealed metamaterial does not reach the same first critical point as the other samples shown in Figure 4d that exhibit mode B collapse. This shows that the behavior of the sample can transition between collapse modes during compression by adjusting the internal pressure. This principle of changing the behavior in real time is further explored in Section 4.

3.3. Buckling Analysis Using Finite Element Simulation

Numerical simulations are used to determine the collapse behavior of material samples over a wide range of geometric parameters. The simulations are completed using FE models in ABAQUS CAE. A two-step simulation is used: first, a static general step where pressure is applied to the inner cavities, then a buckling analysis is performed for biaxial compression. A 2D model is used due to the constant cross section of the structure. The material is modeled using a hyperelastic, neo-Hookean material model with Young's modulus 485 kPa and a Poisson's ratio of 0.499. The model loading conditions are similar to the boundaries of the experimental setup. By using a buckling analysis, the collapse mode (A or B) can be identified. The collapse mode for each combination of geometric parameters and applied pressure is observed as the first reported eigenmode.

3.4. Parametric Study of Geometric and Ligament Ratios

When plotted as a function of the geometric ratio and ligament ratios, Equation (11) results in a surface indicating the necessary pressure to change from collapse mode A to B. This surface is shown in **Figure 5**a. The area below the surface (dark blue) indicates that a material with an applied pressure ratio less than a value on the surface will exhibit mode A collapse, while above the surface (light blue) indicates mode B collapse. As expected, materials with low geometric ratios require relatively low pressures to change from mode A to B, since low geometric ratios

ADVANCED
SCIENCE NEWS
www.advancedsciencenews.com

ADVANCED
ENGINEERING
MATERIALS
www.aem-journal.com

Figure 5. Comparison of the analytical, experimental, and simulated results. a) 3D phase diagram showing boundary surface (black). Below the surface (dark blue) indicates mode A, above (light blue) indicates mode B. b) 2D slice at geometric ratio of 1.67 comparing model to experimental (yellow squares) and numerical results (triangles for mode A, circles for mode B). Shaded regions are determined by the analytical model (black line).

result in thin ligaments. As the geometric ratio increases, the pressure threshold for mode conversion also rises. The model predicts a maximum pressure ratio threshold for ligament ratios between 0.25 and 0.4. As the ligament ratio increases, the pressure threshold decreases to vanishing values. Above a certain ligament ratio, mode B is achieved without any applied pressure.

The trends seen in the analytical model are represented in both the experimental and numerical results. To compare the results, a 2D cross section of the surface of Equation (11) at a geometric ratio of 1.67 is shown in Figure 5b. The experimental results are indicated by yellow squares along with a photograph showing the resulting collapse shape. The FE results for mode A are represented by the dark blue triangle, and mode B is represented by light blue circles. The solid black line represents the predicted boundary by the analytical model. Simulations are also performed for geometric ratios between 1.5 and 1.75 as reported in Figure S2 in Supporting Information.

Both the experimental and numerical models show good agreement with the boundary predicted by the analytical model with small variation at the ligament ratio extremes. For smaller values of ligament ratio such as $\lambda < 0.25$, the simulated results predict a lower pressure threshold than Equation (11). This variation may derive from the assumption that the material is sufficiently stiff so that the applied pressure does not cause any extension of the ligaments. At small ligament ratios, the A-ligaments become considerably thin; therefore, the pressure to the inner cavities causes expansion, which is captured in the FE numerical model but neglected in the analytical model. As the ligament ratio increases, Equation (11) predicts a pressure threshold higher than the simulated results. The analytical model is developed with an assumption of pure rotation at the center of the ligament which becomes less valid as the thickness of the ligament increases. While consideration of these factors may slightly increase the accuracy of the model, the results here indicate that the simplified modeling approach can be used to enable the design of bimodal metamaterials with pneumatic actuation.

While each sample presented in this work has uniform ligament sizes and applied pressure, the behavior explored here can be extended through the use of functional grading and multichannel pressure control. This can lead to a structure composed of independently controlled sections with tunable responses to global loading conditions.

This paper focuses on one example of a bimodal hierarchical metamaterial using a modified pattern of rotating squares, yet other geometries may exhibit multimodal behavior through the introduction of cavities that can be controlled through pneumatic pressure. Section S3 in the Supporting Information discusses the kinematic relationships that determine if additional hierarchical cavities of periodic tilings facilitate a multimodal collapse. The Kutzbach–Grübler criteria[37] determines the mobility of closed-loop planar mechanisms. By representing the added hierarchical cavities as planar mechanisms, the criteria can be used to determine if additional degrees of freedom are introduced to the modified tiling. For a triangular tiling like the Kagome lattice Figure S5b, Supporting Information, the additional triangular cavities have no kinematic mobility. Therefore, the modified Kagome lattice does not exhibit multimodal behavior. For a trihexagonal tiling Figure S5c, Supporting Information, the addition of hexagonal voids introduces greater kinematic mobility and therefore leads to multiple collapse modes. Numerical simulations in the Supporting Information Section S3 show how the method of pressurizing the additional cavity to control the collapse mode is applied to the modified trihexagonal pattern. By applying this criterion to other hierarchical geometries, this work presents a general framework to create novel multimodal metamaterials.

## 4. Rapid Tuning of Collapse Behavior with Pneumatic Pressurization

The results shown in Figure 4d and 5b demonstrate the ability of a metamaterial with a given ligament ratio to exhibit either mode A or mode B collapse by applying a constant pressure to the inner cavities. The pressurization is applied before collapse and maintained throughout biaxial compression resulting in two distinct force responses represented by the dark blue (dot dashed) and light blue (dotted) curves in Figure 4d. This behavior shows that

active pressurization before loading can control the deformation modes in a bimodal metamaterial, yet it may be beneficial to be able to change the behavior while the metamaterial is in use. The fully sealed sample shows how gradually changing the internal cavity pressure – namely by a pneumatic spring effect – the collapse behavior can shift during compression. Here, it is shown that by quickly changing the applied pressure during collapse, the mechanical properties and shape reconfiguration of bimodal metamaterials are rapidly tunable in real time.

To demonstrate this high-rate change of mechanical behavior, a sealed sample of the modified square pattern (Section 3.2) with a ligament ratio of 0.6 is biaxially compressed with pressure applied and removed at discrete times during collapse. To control the pressure in the sample, an exhaust valve is added between the pressure regulator and sealed sample as shown in Figure S4 of Supporting Information. When closed, the pressure regulator supplies a constant pressure to the smaller cavities. If the exhaust valve is opened, the applied pressure drops to zero, and air flows out of the cavities. The applied pressure used in the experiment is 8.6 kPa which results in a pressure ratio (p/E) of approximately

0.018 for the silicone rubber (Young's modulus of 485 kPa) used. As seen in Figure 5b, the pressure ratio threshold for $\lambda = 0.6$ to exhibit mode B collapse is about 0.008. By selecting a value higher than the threshold, the transition from unpressurized to pressurized causes a rapid change of mechanical behavior associated with crossing the pressure ratio threshold by a large margin. The sample is compressed using the biaxial frame described in Section 2.2 with a vertical displacement rate of 2 mm min^{-1} for 20 mm and then unloaded at the same rate.

Figure 6a shows the reaction force from the sample in time, and Figure 6b shows the corresponding mechanical properties including the hysteresis loops recorded from the loading–unloading cycle. The dark blue lines show the force response of the sample with no applied pressure which exhibits mode A collapse. The light blue line is the response of the sample with a constant applied pressure that shows collapse mode B. The green line (solid) shows the sample with no initial pressurization, and pressure is applied at 250 s. Figure 6c shows photographs before and after the pressure is applied, as well as the final collapsed state Movie S1, Supporting Information, shows
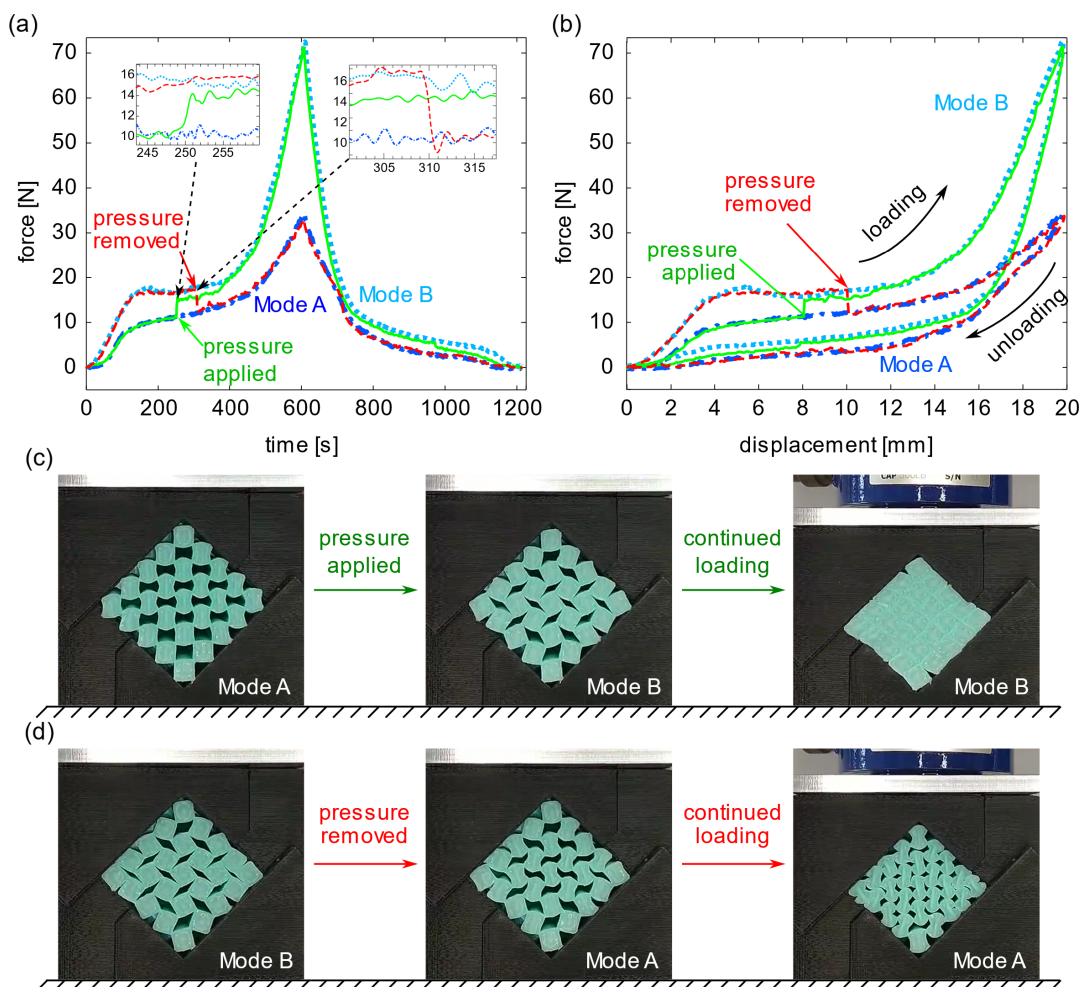
Figure 6. Dynamic force change of pressurized bimodal metamaterial under biaxial compression: a) reaction force in time, and b) force–displacement curves for no applied pressure (dark blue-dot dashed), constant pressure (light blue-dotted), pressure applied during collapse (green solid), and pressure removed during collapse (red dashed). The inset graphs magnify the moment the pressure is applied and removed. Photographs of a sample before and after the pressure is applied c) and a sample when pressure is removed d).

comparable animations of the collapse behavior from mode A to B and from mode B to A by respective application and release of the applied pressure.

For the sample that begins with mode A behavior, the photographs and loading curves in Figure 6 show that the sample initially exhibits mode A collapse. Yet after the pressurization, the behavior snaps to mode B collapse within 1 s. This is seen as the green solid curve initially follows the dark blue curve (mode A) loading curve but sharply jumps to follow the light blue loading curve (mode B) at the moment pressure is applied (250–251 s). After the pressurization, the sample continues to exhibit mode B behavior up to the end of the first stage of collapse as seen in the rightmost photograph of Figure 6c. Conversely, the red (dashed) loading curve shows an initially pressurized specimen with the pressure removed at 310 s. Figure 6d shows the sample before and after the pressure is removed. In this case, the material initially collapses with mode B behavior and snaps to mode A within a second of the removal of the pressure (310–311 s). After the pressure is removed, the sample continues to exhibit mode A collapse for the rest of the loading cycle. The inset graphs in Figure 6a highlight the time when the pressure is applied and removed. As seen by the steep jump in both the dashed curves, the jump from one mode to another occurs in approximately 1 s.

With relatively low pressure, the collapse behavior of bimodal metamaterials can be quickly tuned by exactly switching between two modal responses and mechanical properties. The ability to rapidly switch to predictable shapes with defined mechanical behavior enables potential application of pneumatic multimodal metamaterials in areas such as reconfigurable materials and mechanological systems. In soft robotics, these metamaterials could allow for a tunable robot to human interface. By adjusting the mechanical properties of the metamaterial, engineers can quickly control the amount of force a robot can apply to a user which can lead to safer human–robot collaborations.[38]

5. Conclusions

This research finds that pneumatic pressurization in a new class of bimodal hierarchical mechanical metamaterials can give rise to high-rate change of mechanical behavior through combined active and passive control. This outcome is associated with exploiting a bifurcation between two configurational modes that complete to be realized within a range of strategic design parameter ratios. The approaches outlined in this work lay a foundation for the design and analysis of other multimodal metamaterials. Through analytical modeling, we articulate the boundary between the collapse modes as functions of pneumatic pressurization and cross-sectional ligament thicknesses. Numerical and experimental studies confirm this demarcation and explore the extensibility of the simplified analytical model to more extreme metamaterial geometries. This framework may be explored through other hierarchical metamaterial cross sections according to the realization of new kinematic mobility via the Kutzbach–Grübler criteria. This research therefore identifies means to exploit a wide range of periodic metamaterial networks for high-rate pneumatic actuation via multimodal mechanical design principles.

Conflict of Interest

The authors declare no conflict of interest.

Data Availability Statement

The data that support the findings of this study are available from the corresponding author upon reasonable request.

[1] J. Shim, S. Shan, A. Košmrlj, S. H. Kang, E. R. Chen, J. C. Weaver, K. Bertoldi, *Soft Matter* **2013**, *9*, 8198.

[2] K. K. Saxena, R. Das, E. P. Calius, *Adv. Eng. Mater.* **2016**, *18*, 1847.

[3] X. Tan, S. Chen, B. Wang, J. Tang, L. Wang, S. Zhu, K. Yao, P. Xu, *Extreme Mech. Lett.* **2020**, *41*, 100990.

[4] C. N. Layman, C. J. Naify, T. P. Martin, D. C. Calvo, G. J. Orris, *Phys. Rev. Lett.* **2013**, *111*, 024302.

[5] X. Tan, B. Wang, Y. Yao, K. Yao, Y. Kang, S. Zhu, S. Chen, P. Xu, *Mater. Lett.* **2020**, *262*, 127072.

[6] R. L. Harne, Z. Wu, K. W. Wang, *J. Mech. Des.* **2016**, *138*, 021402.

[7] N. Hu, R. Burgueño, *Smart Mater. Struct.* **2015**, *24*, 063001.

[8] H. Yang, L. Ma, *J. Mater. Sci.* **2019**, *54*, 3509.

[9] R. Poon, J. B. Hopkins, *Adv. Eng. Mater.* **2019**, *21* 1900802.

[10] Y. Li, Q. Zhang, Y. Hong, J. Yin, *Adv. Funct. Mater.* **2021**, *31* 2105641.

[11] D. M. Correa, T. Klatt, S. Cortes, M. Haberman, D. Kovar, C. Seepersad, *Rapid Prototyping J.* **2015**, *21*, 193.

[12] S. Shan, S. H. Kang, J. R. Raney, P. Wang, L. Fang, F. Candido, J. A. Lewis, K. Bertoldi, *Adv. Mater.* **2015**, *27*, 4296.

[13] P. Vuyk, R. L. Harne, *Extreme Mech. Lett.* **2020**, *37*, 100682.

[14] B. Haghpanah, L. Salari-Sharif, P. Pourrajab, J. Hopkins, L. Valdevit, *Adv. Mater.* **2016**, *28*, 7915.

[15] C. El Helou, P. R. Buskohl, C. E. Tabor, R. L. Harne, *Nat. Commun.* **2021**, *12*, 1633.

[16] Z. Meng, C. Chen, T. Mei, Y. Lai, Y. Li, C. Q. Chen, *Extreme Mech. Lett.* **2021**, *43*, 101180.

[17] K. Bertoldi, *Annu. Rev. Mater. Res.* **2017**, *47*, 51.

[18] K. Bertoldi, M. C. Boyce, S. Deschanel, S. M. Prange, T. Mullin, *J. Mech. Phys. Solids* **2008**, *56*, 2642.

[19] K. Bertoldi, P. M. Reis, S. Willshaw, T. Mullin, *Adv. Mater.* **2010**, *22*, 361.

[20] J. N. Grima, A. Alderson, K. E. Evans, *Phys. Status Solidi B* **2005**, *242*, 561.

**ADVANCED
SCIENCE NEWS**

www.advancedsciencenews.com

**ADVANCED
ENGINEERING
MATERIALS**

www.aem-journal.com

[21] Y. Tang, J. Yin, *Extreme Mech. Lett.* **2017**, *12*, 77.

[22] J. T. B. Overvelde, S. Shan, K. Bertoldi, *Adv. Mater.* **2012**, *24*, 2337.

[23] J. T. B. Overvelde, J. C. Weaver, C. Hoberman, K. Bertoldi, *Nature* **2017**, *541*, 347.

[24] Y. Jiang, Y. Li, *Adv. Eng. Mater.* **2016**, *19*, 1600609.

[25] C. El-Helou, R. L. Harne, *Adv. Eng. Mater.* **2019**, *21*, 1900807.

[26] J. T. B. Overvelde, T. A. de Jong, Y. Shevchenko, S. A. Becerra, G. M. Whitesides, J. C. Weaver, C. Hoberman, K. Bertoldi, *Nat. Commun.* **2016**, *7*, 10929.

[27] C. Coulais, A. Sabbadini, F. Vink, M. van Hecke, *Nature* **2018**, *561*, 512.

[28] N. An, A. G. Domel, J. Zhou, A. Rafsanjani, K. Bertoldi, *Adv. Funct. Mater.* **2019**, *30* 1906711.

[29] A. Bossart, D. M. J. Dykstra, J. van der Laan, C. Coulais, *Proc. Natl. Acad. Sci.* **2021**, *118*, e2018610118.

[30] R. Hedayati, S. Lakshmanan, *Materials* **2020**, *13*, 1456.

[31] Q. Pan, S. Chen, F. Chen, X. Zhu, *Sci. China Technol. Sci.* **2020**, *63*, 2518.

[32] Y. Chen, L. Jin, *Extreme Mech. Lett.* **2018**, *23*, 55.

[33] B. Mosadegh, P. Polygerinos, C. Keplinger, S. Wennstedt, R. F. Shepherd, U. Gupta, J. Shim, K. Bertoldi, C. J. Walsh, G. M. Whitesides, *Adv. Funct. Mater.* **2014**, *24*, 2163.

[34] N. Kidambi, V. Agarwal, T. N. Tallman, K. W. Wang, in *Proc. of the Active and Passive Smart Structures and Integrated Systems Conf., Inter. Society for Optics and Photonics*, SPIE, Bellingham, Washington **2020**, p. 1137624.

[35] C. Nikhare, M. Weiss, P. D. Hodgson, *J. Manuf. Processes* **2017**, *28*, 1.

[36] L. L. Howell, *Compliant Mechanisms*, Wiley, New York **2001**.

[37] G. Gogu, *Mech. Mach. Theory* **2005**, *40*, 1068.

[38] S. Robla-Gómez, V. M. Becerra, J. R. Llata, E. Gonzalez-Sarabia, C. Torre-Ferrero, J. Perez-Oria, *IEEE Access* **2017**, *5*, 26754.

Rapid pneumatic control of bimodal, dual-stage mechanical metamaterials

Lance P. Hyatt and Ryan L. Harne*

Department of Mechanical Engineering, Pennsylvania State University, University Park, PA 16802 USA

*Corresponding author: ryanharne@psu.edu

1   Formulation of the pseudo-rigid-body model

The principle of minimum potential energy is used to determine the critical buckling load for each collapse mode. Using the pseudo-rigid-body model (PRBM) of a unit cell as seen in Figs. 3c,e, the ligaments are modelled as revolute joints with torsional springs. The torsional spring constants are K_A and K_B. The remainder of the cell is assumed to be rigid. The approximate total potential energies for mode A (Π_A) mode B (Π_B) with respect to change of angle are

$$\Pi_A = 4\left[\frac{1}{2}K_A\left(\Delta\theta_A\right)^2\right] - 4w\left(F - pr_1\right)\left(r_2 - r_2\cos\Delta\theta_A\right) \tag{S1}$$

$$\Pi_B = 4\left[\frac{1}{2}K_B(\Delta\theta_B)^2\right] - 4w\sqrt{2}Fr_3\left(1 - \cos\Delta\theta_B\right) \tag{S2}$$

The principle of minimum potential energy states that in equilibrium

$$\frac{\partial\Pi_A}{\partial\Delta\theta_A} = \frac{\partial\Pi_B}{\partial\Delta\theta_B} = 0 \tag{S3}$$

$$4K_A\Delta\theta_A - 4w\left(F - p\,r_1\right)r_2\sin\Delta\theta_A = 0 \tag{S4}$$

$$4K_B\Delta\theta_B - 4w\sqrt{2}Fr_3\sin\Delta\theta_B = 0 \tag{S5}$$

The critical forces F_{crA} and F_{crB} are found for small deformations ($\Delta\theta_A = \Delta\theta_B = 0$)

$$F_{crA} = \frac{K_A}{wr_2} + p\,r_1 \tag{S6}$$

$$F_{crB} = \frac{K_B}{\sqrt{2}wr_3} \tag{S7}$$

The boundary between mode A and mode B is found when Eqs. S6 and S7 are equal. Solving for pressure yields Eq. 7.

1.1 Determination of the torsional spring constants through numerical simulation

Meng et al. [1] developed a model using dimensional analysis to approximate the torsional spring constant of a thin square ligament subjected to bending between the ligament ends. A constant K_θ is defined by

$$K_\theta = \alpha E w l^2 \tag{S8}$$

where E is the Young's modulus, *w* is the out-of-plane thickness, *l* is the thickness of the ligament, and α is a non-dimensional correction factor. Equation S8 is used here to approximate the spring constants for both the ligament types of the bimodal metamaterial. For the A-ligaments corresponding to collapse mode A as defined in the main text, the spring constant is approximated here to be

$$K_A = \alpha_A E w (\lambda L)^2 \tag{S9}$$

Similarly, the stiffness of B-ligaments is approximated as

$$K_B = \alpha_B E w L^2 \tag{S10}$$

To determine the value of the correction factor, a finite element (FE) model is created for each ligament. The FE analysis is conducted using ABAQUS general static simulations. The material is modeled using a hyperelastic, Neo-Hookean material model with a Young's modulus of 485 kPa, and a Poisson's ratio of 0.499. A 2D model is used because of the constant cross-section of the ligaments. The model is meshed with CPS4R elements. The geometries of the ligaments are shown in Figs. S1a and S1c. Moments M are applied on both ends of the ligament and the resulting rotation of the ligaments is indicated by the angle θ. By assuming that the ligaments behave like linear torsional springs for small angles of deformation, the spring constants can be calculated with the equation

$$K = \frac{M}{\theta} \tag{S11}$$
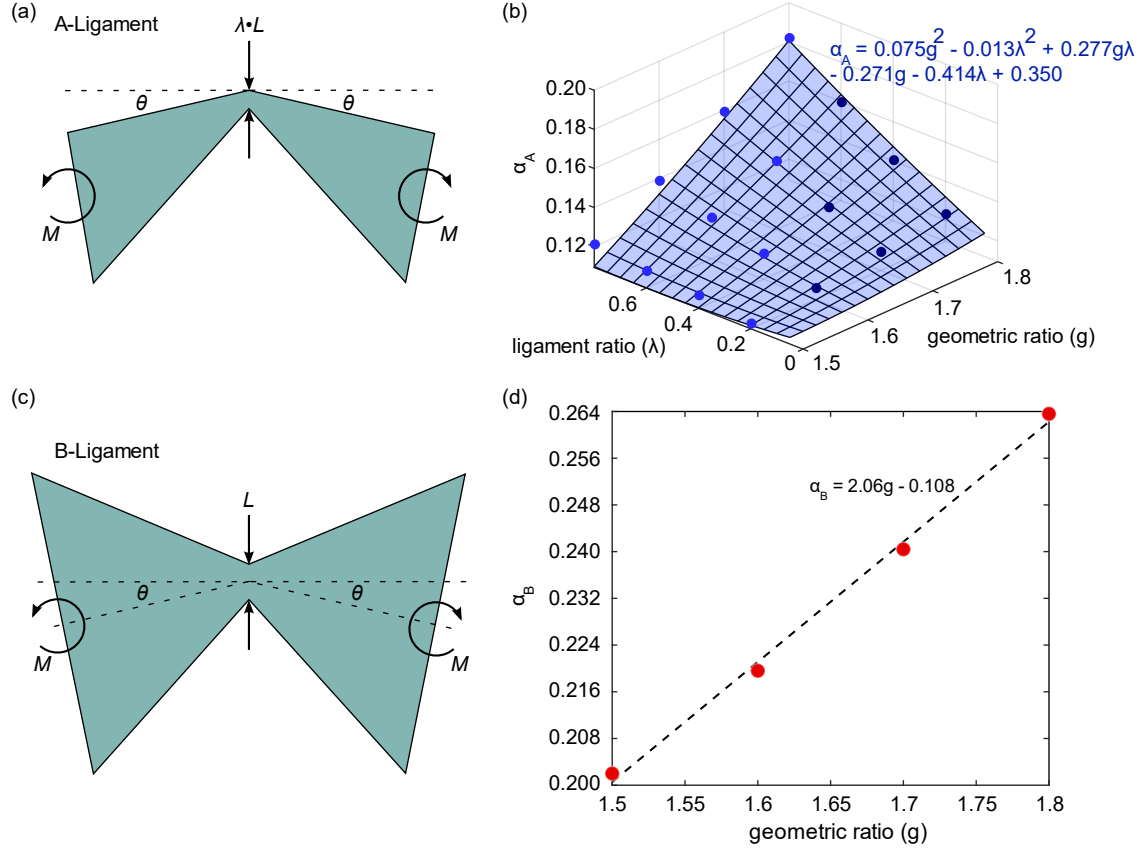
Figure S1. Determination of correction factors through finite element simulation. Hinges are simulated for (a) A-ligaments and (c) B-ligaments. The calculated correction factors from Eqs. (S9) and (S10) (b,d) with curve fit equations.

Using Eqs. (S9)-(S11) the correction factors are found for a range of ligament and geometric ratios. Calculated factors are represented by the data points in Figure S1b and S1d. The correction factor α_A changes with respect to both ratios, while factor α_B only changes with respect to the geometric ratio. A quadratic fit is established to map the surface modeling α_A as a function of both ligament and geometric ratios, and a linear fit is established for α_B as a function of geometric ratio. The curve fit equations are given below.

$$\alpha_A = 0.075g^2 + 0.013\lambda^2 + 0.277g\lambda - 0.271g - 0.414\lambda + 0.350 \tag{S12}$$

$$\alpha_B = 2.06g - 0.108 \tag{S13}$$

These functions are used in the comparison of the analytical model to the experimental and numerical results in Sec. 3 of the main text.

1.2 Expanded parametric study of geometric and ligament ratios

Equation 11 relates the ratio of the applied pressure and the modulus of elasticity (p / E) to the ligament ratio λ and the geometric ratio g. The resulting surface from Eq. 11 is shown in Fig. S2a. Numerical simulations as described in Section 3.3 are performed for geometric ratios of 1.5, 1.63, 1.7, and 1.75 to determine the accuracy of the analytical model. These ratios are indicated by the planar cross-sections outlined in white in Fig. S2a. These cross-sections are displayed as 2D graphs in Fig. S2b. The dark blue triangles represent simulations exhibiting Mode A collapse and the light blue circles represent simulations with Mode B collapse.
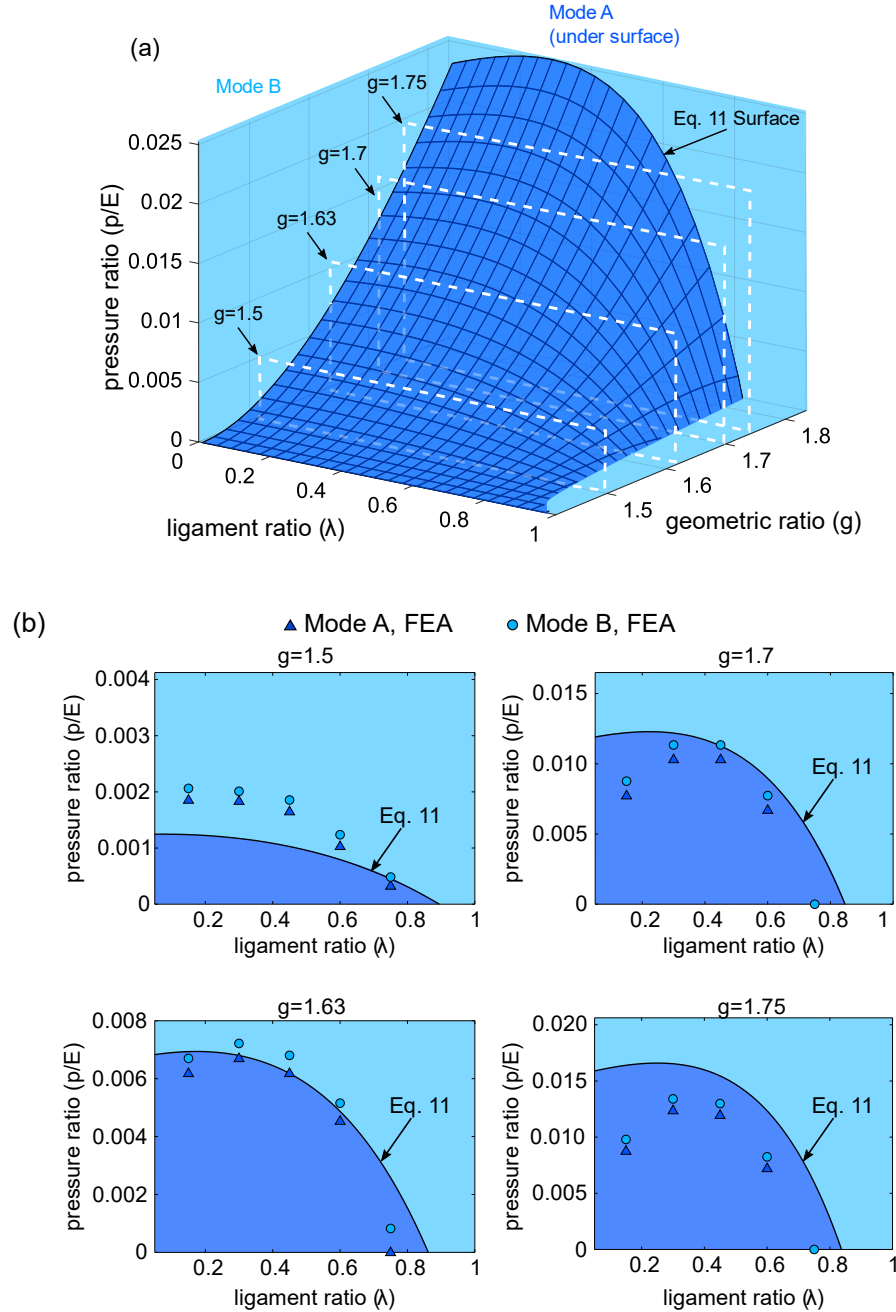
Figure S2. Comparison of the analytical model to simulated results for different geometric ratios. (a) Phase diagram with profiles of fixed geometric ratio for assessment in (b). (b) Numerical simulation results are shown with the triangles (Mode A) and circles (Mode B), and the black line shows the analytical threshold determined by Eq. 11.

This parametric study more broadly investigates the influences of change in geometric ratio and the ligament ratio. A broader understanding of the influence of the A-ligaments and B-ligaments on the modal response is therefore sought. Equation S12 shows how the correction factor and subsequent torsional spring constant of A-ligaments vary with both ligament and geometric ratios. In contrast, Eq. S13 shows that the torsional spring constant of B-ligaments only varies with the geometric ratio. Therefore, the changes in the pressure threshold of the phase diagram with changing ligament ratios are only caused by the changing A-

ligaments. The change in pressure threshold as the geometric ratio increases is a result of both the B-ligaments and A-ligaments.

The model shows good agreement with simulated results for geometric ratios between 1.63 and 1.7. For geometric ratios below 1.63, the model underpredicts the pressure needed to change mode behavior. By contrast, for geometric ratios above 1.7, the model overpredicts pressures required to tailor collapse mode response. These differences are most likely due to the assumptions made in the development of the model as discussed in Sec. 3.4.

2   Specimen fabrication and experimental setup

The open samples shown in Fig 1d,e are made of silicone rubber (Smooth On Mold Star 15S) cast in 3D-printed (Creality Ender 3 V2) molds made of polylactic acid (PLA). The material is cured at room temperature and room pressure. The samples are designed with side lengths of 6 mm and geometric ratios of 1.67 as seen in Fig. 1d,e. To show the two collapse modes, ligament ratios of 0.3 and 1.2 are chosen. Both samples have a constant cross-section and out-of-plane thickness w of 25 mm. The material has a Young's modulus of 485 kPa, measured empirically.

The sealed material samples are created with a multi-step casting process using the same silicone rubber. Three molds are 3D printed for the three parts seen in Fig. S3a. The first mold is the negative of the sample geometry. The second mold is for a cap with a single channel that connects all of the smaller cavities in the sample. The last mold is for a conical section with a small hole in the center. Once the three parts are cured and removed from the mold, they are assembled by applying a small portion of uncured rubber between the mating surfaces creating a single sealed structure as seen in Fig. S3b. After assembly, the smaller cavities are sealed on one end and connected by a single channel as seen by the cross-section in Fig. S3c. The resulting monolithic elastomeric mechanical metamaterial can be pressurized through the conical section. The specimen can then be connected to an air supply by inserting a 1/4" polyethylene (PE) tube into the hole in the conical section. The resistance from insertion of the tube is found to be sufficient to prevent air leakage given the pneumatic pressures used here in this report.
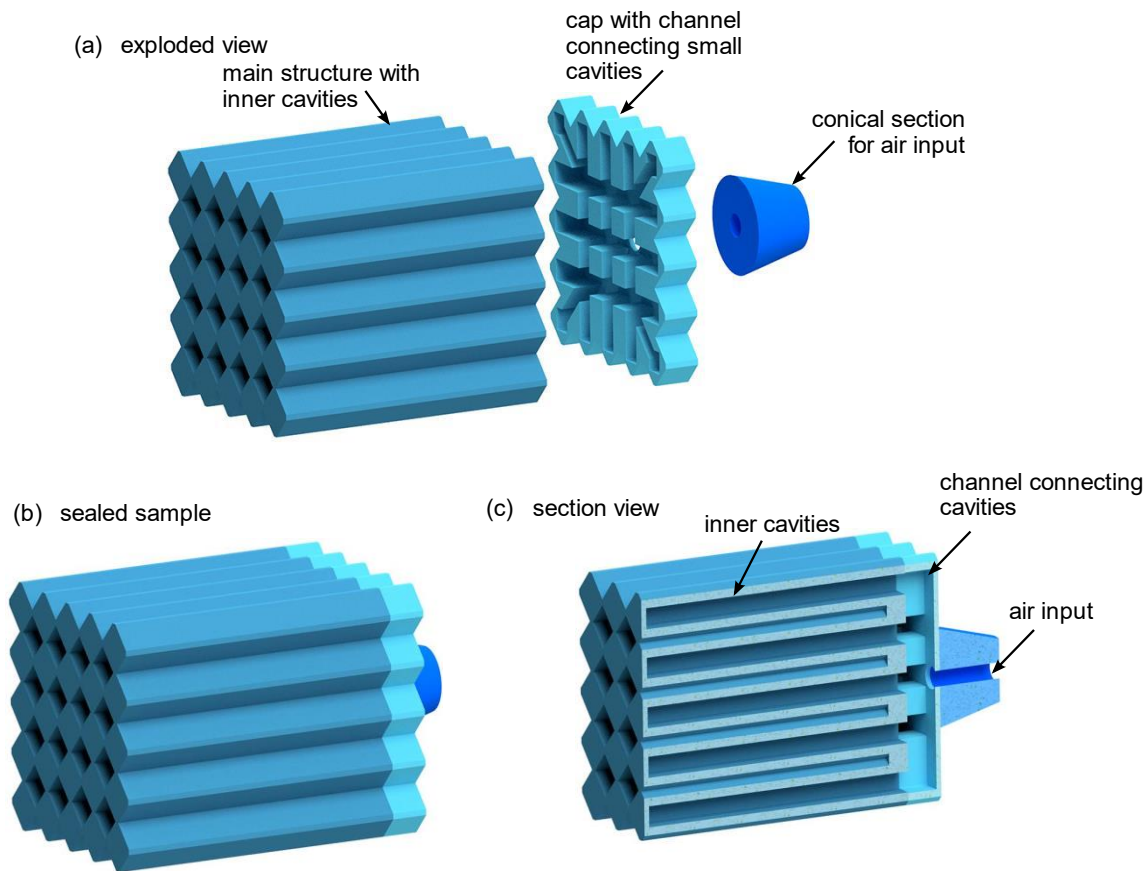
Figure S3. Diagram of sealed sample fabrication. (a) Exploded view showing individual molded pieces. (b) Assembled sample and section view (c) showing inner cavities.

## 2.1 Experimental setup of pressurization changes during collapse

To adjust the pressure during collapse, a valve system is added between the pressure regulator and the molded sample as seen in Fig. S4. The regulator is set at a constant pressure of 8.6 kPa and the exhaust valve is closed to apply pressure and opened to remove pressure. This allows for rapid switching between pressurization states as seen in Sec 4 of the main text.
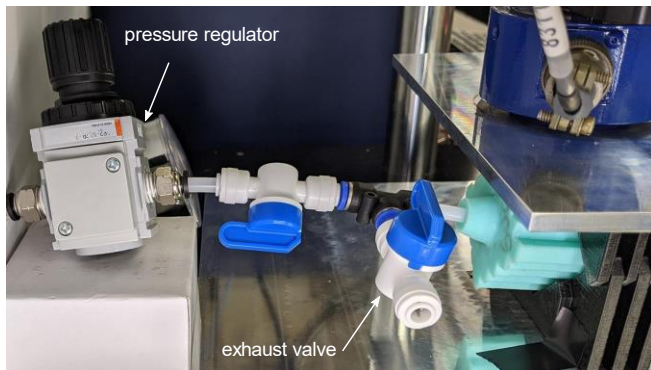
Figure S4. Photo of experimental setup for real-time pressure changes. Exhaust valve allows for rapid application or removal of pressure input

3 Application of pneumatic control to other periodic tilings

A range of periodic tilings of kinematically reconfigurable geometries that can reach a fully compact configuration have been studied [2] [3]. The main text of this report studies one such geometry within the new framework of dual-stage voids and dual-stage collapse shown again in Fig. S5a. Two more of such reconfigurable geometries are examined here to demonstrate how the introduction of pressurized cavities is applicable to control multi-modal collapse of a wider range of elastomeric mechanical metamaterials. The first sample is a triangular tiling referred to as a Kagome lattice (Fig. S5b) and the second pattern is a trihexagonal tiling (Fig. S5c).
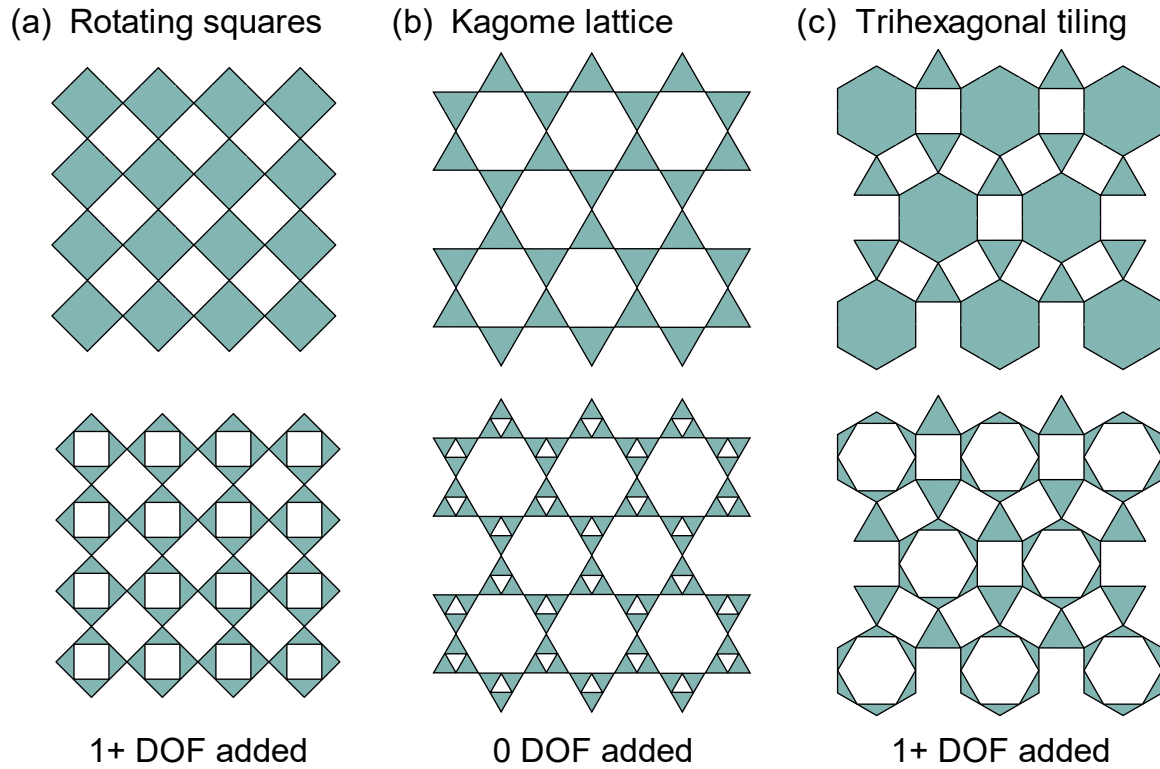
Figure S5. Selection of geometries capable of reaching a fully compact configuration (top) with additional hierarchical cellular voids (bottom). (a) Rotating squares from main text, (b) triangular tiling (Kagome lattice), and (c) trihexagonal tiling.

3.1 Kagome lattice

Under uniaxial compression, the original Kagome lattice seen in Fig. S5b reaches a fully compact configuration with one soft mode of deformation. If a smaller triangular cavity is introduced in the center of each individual triangle, no additional modes are introduced. The Kutzbach-Grübler criteria for planar mechanisms [4] can determine the degrees of freedom of a linkage based on the number of links n, the number of lower pairs (such as revolute joints) J_1, and the number of higher pairs J_2 with the equation

$$DOF = 3(n-1) - 2(J_1) - J_2 \tag{S14}$$

By examining the ideal kinematic behavior of the resulting triangular units, the cavity creates a structure of three links connected with three revolute joints (no higher pairs). Equation S14 indicates that there will be no additional degrees of freedom in the added cavity, therefore no additional soft modes are introduced. Thus, the pattern remains monomodal. In contrast, the additional square cavity in Fig. S5a is structure with 4 links and 4 revolute joints. Equation S14 indicates that the square cavity has one DOF. This is reflected by the additional collapse mode explored in the main text.

3.2 Trihexagonal tiling

Like the Kagome lattice, the trihexagonal tiling in Fig. S5c reaches a fully compact configuration under uniaxial compression. Yet, when another hexagonal cavity is introduced in the center of each hexagonal tile, additional collapse modes are in fact possible. The resulting hexagonal unit has six additional joints that add multiple degrees of freedom. This translates to additional soft modes of collapse. Like the modified rotating squares pattern, the activation of the modes in the trihexagonal pattern depends on the ligament ratios and can be further controlled with pneumatic pressure.

The trihexagonal pattern is described by the side length of the square cavities s, a radial ratio that relates the distance from the center of the squares to the center of the hexagonal section r, and a ligament ratio λ similar to the rotating squares structure. The parameters are visualized on a unit cell in Fig. S6a. The two collapse modes are observed in experimental samples with ligament ratios of 1.6 and 2.4 in Fig. S6c-d. These samples are fabricated by the same method and material as described in Sec. S2. Mode A occurs when the ligaments surrounding the hexagonal cavity deflect, and mode B occurs when the square cavities collapse like the original trihexagonal pattern with no added cavity. These modes can be controlled either by changing the ligament ratio or by adding pneumatic control.

To determine the relationship between the ligament ratio and applied pressure, FE simulations are conducted. A 2D model is created with the same number of cavities as the specimens in Fig. S6c-d. The simulations use the same material properties outlined in Section 3.3 of the main text (Neo-Hookean material model with Young's modulus of 485 kPa and Poisson's ratio of 0.499). The models are fixed on the bottom edges and a uniaxial force is applied on the top edges to match the experimental conditions. Similar to the simulations of the rotating squares pattern, a two-step analysis is used. Pressure is first applied to the hexagonal cavities in a static general step, and then a buckling analysis is performed for uniaxial compression in the next step. The results for a sample with a radial ratio of 1.5 are shown in Fig. S6b for a range of ligament ratios. The boundary shown (black line) is estimated based on the simulation results. While this study is limited to only one radial ratio, the applied pressure is anticipated to be a function of both radial and ligament ratios for the same reasons discussed in Sec. 3. This investigation exemplifies how the principle of pneumatic and geometric control of collapse modes is manifest in other periodically tiled geometries.
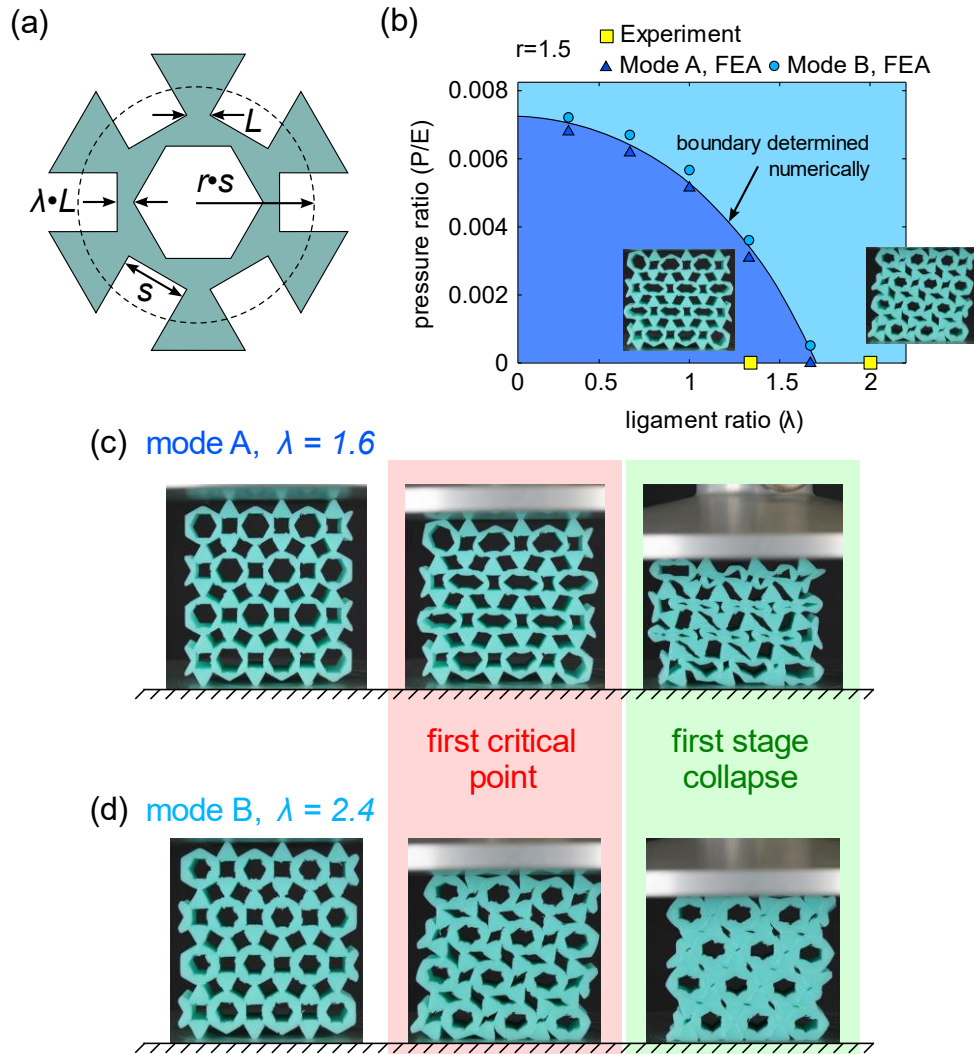
Figure S6. Trihexagonal tiling description and results. (a) Diagram showing design parameters. (b) Numerical results showing different deformation modes (triangles for mode A, circles for mode B), and experimental results (yellow square). Photographs showing two deformation modes under uniaxial compression based on ligament ratio for (c) mode A and (d) mode B.

4   Movie description

Movie S1 shows the switching behavior of the pressurized dual-stage mechanical metamaterial. At left is an unpressurized sample with Mode A behavior that transitions to Mode B behavior when pressure is applied. At right is shown an initially pressurized sample with Mode B behavior that transitions to Mode A behavior when pressure is removed.

References

[1] Z. Meng, C. Chen, T. Mei, Y. Lai, Y. Li, C.Q. Chen, *Extreme Mechanics Letters* **2021**, *43*, 101180.

[2] J. Shim, S. Shan, A. Košmrlj, S.H. Kang, E.R. Chen, J.C. Weaver, K. Bertoldi, *Soft Matter* **2013**, *9*, 8198-8202.

[3] J.N. Grima, A. Alderson, K.E. Evans, *Physica Status Solidi B* **2005**, *242*, 561-575.

[4] G Gogu, *Mechanism and Machine Theory* **2005**, *40*(9),.